JOURNAL OF GEOPHYSICAL RESEARCH, VOL. 111, C03016, doi:10.1029/2005JC003004, 2006

Drift and mixing under the ocean surface: A coherent one-dimensional description with application to unstratified conditions

Nicolas Rascle,[1] Fabrice Ardhuin,[1] and Eugene A. Terray[2]

Received 15 April 2005; revised 6 December 2005; accepted 21 December 2005; published 24 March 2006.

[1] Waves have many effects on near-surface dynamics: Breaking waves enhance mixing, waves are associated with a Lagrangian mean drift (the Stokes drift), waves act on the mean flow by creating Langmuir circulations and a return flow opposite to the Stokes drift, and, last but not least, waves modify the atmospheric surface roughness. A realistic ocean model is proposed to embrace all these aspects, focusing on near-surface mixing and surface drift associated with the wind and generated waves. The model is based on the generalized Lagrangian mean that separates the momentum into a wave pseudomomentum and a quasi-Eulerian momentum. A wave spectrum with a reasonably high frequency range is used to compute the Stokes drift. A turbulent closure scheme based on a single evolution equation for the turbulent kinetic energy includes the mixing due to breaking wave effects and wave-turbulence interactions. The roughness length of the closure scheme is adjusted using observations of turbulent kinetic energy near the surface. The model is applied to unstratified and horizontally uniform conditions, showing good agreement with observations of strongly mixed quasi-Eulerian currents near the surface when waves are developed. Model results suggest that a strong surface shear persists in the drift current because of the Stokes drift contribution. In the present model the surface drift only reaches 1.5% of the wind speed. It is argued that stratification and the properties of drifting objects may lead to a supplementary drift as large as 1% of the wind speed.

Citation: Rascle, N., F. Ardhuin, and E. A. Terray (2006), Drift and mixing under the ocean surface: A coherent one-dimensional description with application to unstratified conditions, *J. Geophys. Res.*, *111*, C03016, doi:10.1029/2005JC003004.

1. Introduction

[2] The ocean surface is where the vast majority of marine activities take place, and different dynamical descriptions have been invoked to describe the 100 m that straddle both sides of the air-sea interface. Different solutions have been developed for applications such as wave forecasting for safety at sea [e.g., *Komen et al.*, 1994], forecasting of drift for search and rescue or pollution mitigation [e.g., *Youssef and Spaulding*, 1993], or modeling of the general ocean circulation with applications to climate studies [e.g., *Semtner*, 1995; *Bleck*, 2002].

[3] Unfortunately, these descriptions of the upper ocean are often incoherent, not always based on first principles, and may not give parameters compatible available measurements that could constrain numerical forecasting models. Work for each of the three applications listed above have often focused on one key parameter, the significant wave height H_s, the surface drift current $U_{\varsigma=0}$, or the mixed layer temperature T_s. The advent of the Global Ocean Observing System (GOOS) and efforts toward operational modeling of the ocean on global and regional scales are good opportunities for finally achieving a common description of the ocean interface that would involve all the relevant dynamic processes: geostrophic currents, ocean waves, tides, internal waves, and known turbulent structures such as wind rolls in the atmospheric boundary layer and both breaking waves and Langmuir circulations in the ocean mixed layer [*Ardhuin et al.*, 2005]. Many good fundamental contributions have studied one or two of these processes, including joint effects of wave motion and mean currents [e.g., *Weber*, 1981; *Jenkins*, 1987], wave breaking, and Langmuir circulations' effects on upper ocean mixing [*Agrawal et al.*, 1992; *Craig and Banner*, 1994; *Thorpe et al.*, 2003; *Mellor and Blumberg*, 2004].

[4] A recent convergence of different approaches to the upper ocean dynamics shows a clear inconsistency. *Mellor and Blumberg* [2004] demonstrated that a parameterization for the strong mixing due to wave breaking, previously observed by *Agrawal et al.* [1992] and others, leads to improved hindcasts of mixed layer depth and temperature of the classic data set from the Gulf of Alaska station Papa. This strong mixing also leads to a rather uniform Eulerian current profile, which has to be small because the depth-integrated transport is the known Ekman transport. *Mellor and Blumberg* [2004] found surface currents less than 0.6% of the wind speed. Such a value of the Eulerian current may

[1]Centre Militaire d'Océanographie, Service Hydrographique et Océanographique de la Marine, Brest, France.
[2]Department of Applied Ocean Physics and Engineering, Woods Hole Oceanographic Institution, Woods Hole, Massachusetts, USA.

0148-0227/06/2005JC003004$09.00

be larger than the quasi-Eulerian current observed by *Santala and Terray* [1992], but it is paradoxically small for experts in the forecasting of surface drift, for whom it is well established that the drift velocity is often close to 2 or 3% of the wind speed at 10 m, U_{10} [*Spaulding*, 1999]. Both a strong mixing and a strong velocity shear at the surface should be obtained when surface waves are accounted for in a consistent way, including both wave breaking and wave-induced Stokes drift.

[5] The goal of the present paper is to evaluate how well a simple but coherent model of the upper ocean performs in terms of drift velocities, Eulerian velocities, eddy viscosities and turbulent dissipation. Since waves are clearly an important part of the oceanic mixed layer, we shall also explore which wave parameters are important and how the mixed layer is modified. In particular the effect of the Hasselmann force [*Hasselmann*, 1970] that was reported to be significant by *Lewis and Belcher* [2004] is reexamined with a realistic parameterization of near-surface mixing. The present paper focuses on conditions that are statistically stationary and homogenous in the horizontal dimensions. The wave forcing and resulting wave properties are described in section 2. These drive a model for turbulent and mean Eulerian properties as described in section 3. That model is based on the approximation to second order in the wave slope of the generalized Lagrangian mean (GLM2 [see *Andrews and McIntyre*, 1978; *Groeneweg*, 1999]) applied to the Reynolds-averaged Navier-Stokes (RANS) equations. This GLM2-RANS formalism can be obtained by subtracting the wave pseudomomentum from the total momentum equation given by *Mellor* [2003], and it is valid for horizontally uniform conditions. This step, as well as a derivation from the equations of *Andrews and McIntyre* [1978], are described by *Ardhuin* [2005]. The numerical calculations use the computer code of *Craig and Banner* [1994], extended to account for wave effects specific to our GML2-RANS equations. In section 4 the various effects of the waves on the turbulent, Eulerian and Lagrangian properties are compared to observations of turbulent kinetic energy dissipation, quasi-Eulerian, and Lagrangian velocities. Conclusions follow in section 5.

2. Wave Dynamics

2.1. Spectral Wave Evolution

[6] Ocean surface waves, generated by the wind, have a large influence on air-sea fluxes. In particular, waves are generally believed to absorb more than 50% the wind-to-ocean momentum flux τ^a [*Donelan*, 1998; *Banner and Peirson*, 1998]. This large fraction of the wind stress τ^a is the wave-induced stress τ^{in}. However, only a small fraction of τ^{in}, possibly up to 5%, is radiated in the wave field momentum flux, the vast majority is continuously lost by waves as they dissipate, essentially because of wave breaking [*Donelan*, 1998; *Janssen et al.*, 2004; *Ardhuin et al.*, 2004a]. Another effect of interest to coastal oceanographers is that for a given wind speed, τ^a can be increased by as much as a factor of 3 in coastal areas because of the different nature of the wave field [e.g., *Drennan et al.*, 2003; *Lange et al.*, 2004].

[7] Because ocean waves are generated by the wind, many authors have sought a direct parameterization of wave effects from the wind field. However, waves are not uniquely defined by the local wind speed and direction, in particular in coastal areas and marginal seas (like the Mediterranean sea), where wave development is limited by the fetch, but also in the tropics and midlatitudes, where a large part of the wave energy is due to long-period waves (swell) that have propagated from distant storms, sometimes halfway around the Earth [*Snodgrass et al.*, 1966]. In general, one needs to take into account the wave dynamics that are, on these large scales, statistically well defined by the directional wave spectrum $E(k, \theta)$, that distributes over wave numbers k and directions θ the wave energy $E^w = \rho_w g \int E(k, \theta) \mathrm{d}k\mathrm{d}\theta$. The evolution of the spectrum is generally modeled using the energy balance equation [*Gelci et al.*, 1957],

$$\frac{\mathrm{d}}{\mathrm{d}t} E(k,\theta) = S^{\mathrm{in}}(k,\theta) + S^{\mathrm{nl}}(k,\theta) + S^{\mathrm{ds}}(k,\theta) + S^{\mathrm{bot}}(k,\theta), \quad (1)$$

where the Lagrangian time derivative includes propagation effects, and S^{in}, S^{nl}, S^{ds}, and S^{bot} are "source terms" (either positive for true sources or negative for actual sinks) that represent the energy given to the spectral component (k, θ) by the atmosphere, the other wave components, the ocean turbulence in the water column and surface boundary layer, and the bottom boundary layer and sediments, respectively. This equation is easily extended to take into account varying currents [*Komen et al.*, 1994; *White*, 1999]. Each energy source terms can be converted in a momentum source term [e.g., *Phillips*, 1977],

$$\tau^i = \rho_w g \int \frac{S^i(k,\theta)}{C} \mathrm{d}k\mathrm{d}\theta, \quad (2)$$

where C is the wave intrinsic phase speed. Of particular interest will be τ^{in} and $-\tau^{ds}$, the momentum fluxes, per unit surface of the ocean, input to waves from the wind, and delivered to the mean flow by the waves, respectively.

2.2. Stokes Drift

[8] It is also well known that waves possess a pseudo-momentum that is equal to the mass transport velocity or Stokes drift $\mathbf{U}_s$ [e.g., *McIntyre*, 1981]. This drift arises as the wave-induced orbits of particles are not exactly closed. From an Eulerian point of view this drift is zero everywhere below the wave troughs, and the wave-induced mass transport occurs between the deepest troughs and the highest crests. However, such an Eulerian view "diffuses" the air-sea interface over a vertical distance of the order of the significant wave height H_s, which is not practical for investigating the surface gradient of any quantity. We shall thus prefer the Lagrangian point of view [e.g., *Andrews and McIntyre*, 1976] that yields, correct to the second order in the wave slope, the following expression for deep water waves [*Kenyon*, 1969]:

$$\begin{aligned} \mathbf{U}_s(z) &= 2 \int_0^{2\pi} \int_0^{\infty} \mathbf{u}_\theta k \sigma e^{2kz} E(k,\theta) \mathrm{d}k\mathrm{d}\theta \\ &= \frac{2}{g} \int_0^{2\pi} \int_0^{\infty} \mathbf{u}_\theta \sigma^3 e^{2kz} E(k,\theta) \mathrm{d}k\mathrm{d}\theta. \end{aligned} \quad (3)$$

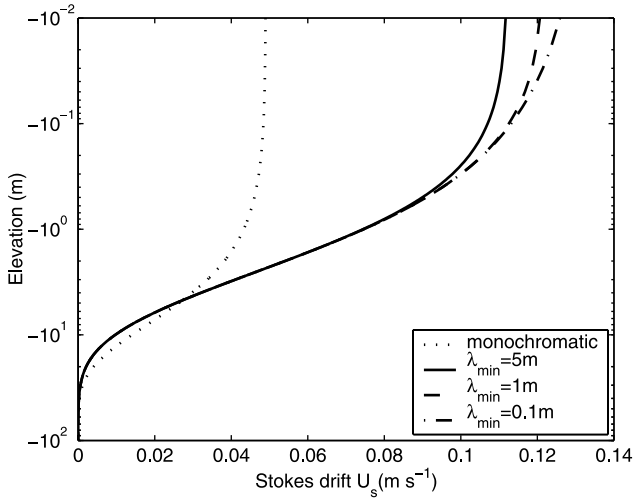

Figure 1. Stokes drift profile for a wind speed U_{10} = 10 m s^{-1}, a fetch larger than 1000 km (fully developed sea) based on the KMC spectrum [*Kudryavtsev et al.*, 1999] and the integral (3). Different profiles are shown that only include wavelengths longer than a minimum value $\lambda_{\min}$. For comparison, the drift due to a single wave component is also indicated. That single component has the same peak wavelength and surface elevation variance (period Tp = 8 s and H_s = 2.8 m) as the wave spectrum.

That expression uses the intrinsic wave radian frequency, as given by the deep water dispersion relation for linear gravity waves, $\sigma = \sqrt{gk}$, g is the acceleration of gravity, and $\mathbf{u}_\theta$ = (cos θ, sin θ) is the unit vector in the direction of propagation. The origin of the vertical coordinate z is at the mean water level.

[9] $\mathbf{U}_s$ is clearly much smaller than the orbital wave velocity, by a factor ε that is the wave slope, typically less than 0.1. $\mathbf{U}_s$ is also strongly sheared at the surface because the contribution of each wave component decays exponentially over its Stokes depth $1/(2k)$, and the high wave number components give a significant contribution to $\mathbf{U}_s$, but near the surface only (Figure 1). Using a spectral shape proposed by *Kudryavtsev et al.* [1999], a wind of U_{10} = 10 m s^{-1} yields a surface drift of $\mathbf{U}_s(z = 0)$ = 0.11 m s^{-1} when only wave components with $2\pi/k > 5$ m are included, whereas all components up to $2\pi/k$ = 0.1 m yield up to 0.13 m s^{-1}. The comparison with a monochromatic component shows the differences between wind sea and swell contributions: The swell-induced Stokes drift at the surface is typically less than 30% of the drift associated with a wind sea of same peak period and significant wave height. A large swell and a wind sea due to a weak wind can then produce surface Stokes drifts of the same order.

[10] The Stokes transport

$$\mathbf{M}^w = \int_{-H}^{0} \mathbf{U}_s \mathrm{d}z = \int_0^{2\pi} \int_0^{\infty} \mathbf{u}_\theta \sigma E(k,\theta) \mathrm{d}k\mathrm{d}\theta \qquad (4)$$

is slightly less influenced by the short (and slower) waves. Nevertheless, the short waves contribute relatively more to $\mathbf{M}^w$ than to the wave energy, as the contribution of each spectral component to $\mathbf{M}^w$ is its surface elevation variance divided by the intrinsic phase speed.

2.3. Practical Calculation of Wave Parameters

[11] Because short waves are important, with $\mathbf{U}_s(z = 0)$ and $\mathbf{M}^w$ proportional to the third and first moments of the frequency spectrum, respectively, a numerical estimation of $\mathbf{U}_s$ based on (3) should use a wave spectrum that is well defined in that range. For general applications using numerical wave models such as WAM [*Wamdi Group*, 1988], the explicitly resolved spectrum can be carefully extended by a high-frequency tail. In the present study, we use the family of spectra proposed for remote sensing applications by *Kudryavtsev et al.* [1999] and governed by the two main parameters that are the wind speed and the stage of wave development. These spectra have been carefully designed to reproduce both the long wave spectrum, with a spectral shape similar to that of *Donelan et al.* [1985] and the short wave spectrum with, in particular, a second moment of the wave number spectrum (or fourth moment of the frequency spectrum) that is well constrained by the optical measurements of the mean sea surface slope by *Cox and Munk* [1954]. One can thus assume that the intermediate third moment that is the Stokes drift is well represented by this model.

[12] These spectra yield values of $\mathbf{U}_s(z = 0)$ that can be larger than typical mean Eulerian currents, with a transport $\mathbf{M}^w$ of the order of the transport at midlatitudes described by *Ekman* [1905], except for short fetches or weak winds (Figure 2). For fully developed waves, $\mathbf{U}_s(z = 0)$ = $0.0125\mathrm{U}_{10}$ is consistent with recent observations of the drift of near-surface clouds of bubbles by J. A. Smith (Observed variability of ocean wave Stokes drift and the Eulerian response to passing groups, submitted to *Journal of Physical Oceanography*, 2005). In the following calculations, the wind speed at 10 m height U_{10} is taken to be in the direction θ = 0. The friction velocity $u_\star$ is determined from U_{10} using *Charnock*'s [1955] expression,

$$U_{10} = \frac{u_{a\star}}{\kappa} \log\left(\frac{z}{z_{a0}}\right), \qquad (5)$$

with

$$z_{a0} = 0.018\, u_{a\star}^2/g, \qquad (6)$$

where z = 10 m, $\tau^a = \rho_w u_\star^2 = \rho_a u_{a\star}^2$ is the wind stress, ρ_w and ρ_a are the densities of water and air. However, it is well established that the sea state and the wind speed are coupled because of the dependence of the wind profile on the roughness of the sea [e.g., *Janssen*, 2004]. *Donelan* [1998] gives a parameterization of z_{a0} that uses the wave age c_p/U_{10} (where c_p is the phase speed at the peak of the wave frequency spectrum) and the significant wave height H_s,

$$z_{a0}/H_s = 1.67 * 10^{-4}\left(U_{10}/c_p\right)^{2.6}. \qquad (7)$$

This effect will be evaluated in section 4.3.

3. Wave-Averaged Mixed Layer Equations

[13] Oceanic motions are separated in three components, mean flow, waves and turbulence. Turbulence is separated from other motions by a an average over flow realizations for given wave phases. The mean flow and wave motions

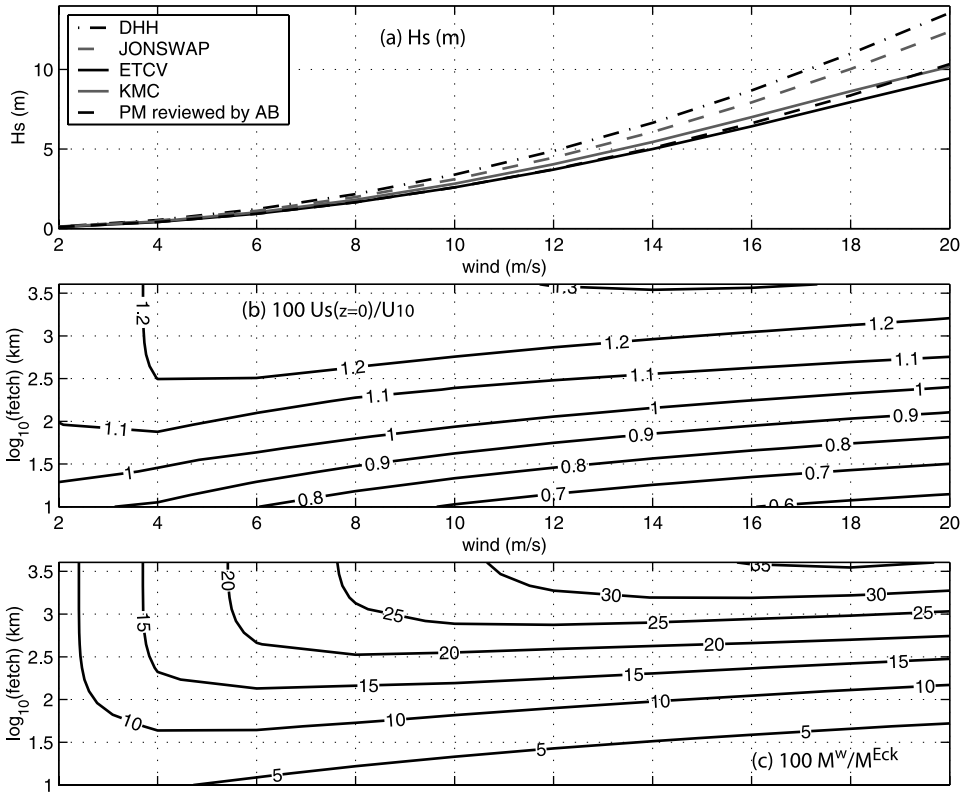

Figure 2. (a) Significant wave height at full development given by several parameterizations of the wave spectrum $E(k, \theta)$: PM, *Pierson and Moskowitz* [1964]; AB, *Alves and Banner* [2003]; DHH, *Donelan et al.* [1985]; JONSWAP, *Hasselmann et al.* [1973]; ETCV, *Elfouhaily et al.* [1997]; KMC, *Kudryavtsev et al.* [1999]. For DHH and JONSWAP, full development is obtained by setting the peak frequency f_p to 0.123 g/U_{10}. (b) Surface Stokes drift as a function of fetch and wind speed U_{10} for the KMC spectrum, expressed as a percentage of U_{10}. (c) Magnitude of the vertically integrated Stokes mass transport $\mathbf{M}^w$ as a function of fetch and U_{10}, expressed as a percentage of the corresponding transport u_*^2/f at midlatitudes [*Ekman*, 1905], with $f = 10^{-4}$.

are then averaged with a Lagrangian mean so that the mean momentum is separated into a mean flow and a wave part. The vertical mean wave momentum is zero while the horizontal total mean momentum $\rho_w \mathbf{U}$ is split in a quasi-Eulerian mean $\rho_w \widehat{\mathbf{u}}$ and a Stokes drift,

$$\mathbf{U} = \widehat{u} + \mathbf{U}_s. \tag{8}$$

[14] This separation comes naturally with the definition of the generalized Lagrangian mean [*Andrews and McIntyre*, 1978]. Please note that $\mathbf{U}$ and $\mathbf{U}_s$ are $\overline{\mathbf{U}}^{\mathbf{L}}$ and $\mathbf{p}$ in their notations and are evaluated at a slightly displaced vertical position [*McIntyre*, 1988]. In measurements this separation may be difficult to achieve [e.g., *Santala and Terray*, 1992; *Hristov et al.*, 1998]. Although the Stokes drift $\mathbf{U}_s$ corresponds to the wave-induced drift that arises from the correlations of wave-induced displacements and wave-induced velocity gradients, as defined by *Phillips* [1977], the quasi-Eulerian velocity $\widehat{\mathbf{u}}$ is more difficult to interpret; $\widehat{\mathbf{u}}$ is the mean velocity of a water particle $\mathbf{U}$ minus $\mathbf{U}_s$, but it is not easily related to Eulerian mean velocities. Another interesting velocity, in particular in remote sensing applications, is the mean of the velocity at a point that is fixed horizontally but moves up and down with the surface elevation ζ. That mean surface velocity is $\widehat{u(\zeta)} = \widehat{\mathbf{u}}\left(\widehat{\zeta}\right) + \mathbf{U}_s\left(\widehat{\zeta}\right)/2$, at second order in the wave slope.

[15] If waves do not interact with the mean flow, $\widehat{\mathbf{u}}$ is the mean flow velocity in the limit of vanishingly small wave amplitudes. However, waves do generally interact with the mean flow.

3.1. Influence of Waves on the Mean Flow

[16] We will use now the equations established by *Ardhuin et al.* [2004b], which are an extension of *Mellor*'s [2003] equations and are valid for horizontally uniform conditions. These are essentially a generalization in three dimensions of the equations of *Garrett* [1976], which are also discussed by *Ardhuin et al.* [2004a]. These equations are also equivalent to the generalized Lagrangian mean equations as given by *Groeneweg and Klopman* [1998], neglecting the modulations of turbulent properties on the scale of the wave phase [*Ardhuin*, 2005]. Following *Ekman* [1905] we assume that the wave, velocity, and turbulent properties are uniform horizontally. In this case, the horizontal momentum conservation simplifies as

$$\frac{\partial \widehat{\mathbf{u}}}{\partial t} = -f \mathbf{e}_z \times (\widehat{\mathbf{u}} + \mathbf{U}_s) + \frac{\partial}{\partial z} \overline{\widehat{\mathbf{u}}' \widehat{w}'} - \mathbf{T}^{ds}(z), \tag{9}$$

with the following boundary conditions, defining our vertical coordinate so that the mean sea level is at $z = \widehat{\zeta} = 0$,

$$\left.\overline{\widehat{\mathbf{u}}'\widehat{w}'}\right|_{z=0} = \frac{\boldsymbol{\tau}^a}{\rho_w} - \frac{\boldsymbol{\tau}^{in}}{\rho_w} \tag{10}$$

and

$$\mathbf{u}|_{z=-H} = 0. \tag{11}$$

Here $\mathbf{T}^{ds}$ is a vertical distribution of τ_{ds}, so that $\tau_{ds} = \rho_w \int_{-H}^{0} T^{ds} dz$.

[17] The influence of the wave motion on the quasi-Eulerian flow appears with the Hasselmann force $-f\mathbf{e}_z \times \mathbf{U}_s$ [*Hasselmann*, 1970] (which combines the Coriolis parameter and the Stokes drift [e.g., *Xu and Bowen*, 1994]) and, in the momentum, transfers from wind to the mean flow. One part of the momentum from the wind goes directly to the mean flow via the surface shear stress $\rho_w \left.\overline{\widehat{\mathbf{u}}'\widehat{w}'}\right|_{z=0}$. It is the direct mean viscous drag of air on water. The other part τ^{in} goes to the wave field, it is the form drag of wind over water plus the wave-induced modulations of the viscous stresses [*Longuet-Higgins*, 1967]. Then the wave field is also dissipated, releasing its momentum to the mean flow. This is the force $-\mathbf{T}^{ds}(z)$. This latter force is constituted by viscous dissipation (the virtual wave stress is part of it), interactions of waves with the turbulence [e.g., *Teixeira and Belcher*, 2002], and wave breaking [*Melville et al.*, 2002].

[18] Observations of wave growth with fetch shows that the momentum retained by the wave field is around 5% of the momentum input (see section 2.1). This leads to the good approximation $\tau^{ds} \simeq -\tau^{in}$. Furthermore, supposing that the momentum is released by the wave field at the surface (i.e., $T^{ds} = \tau^{ds}\,\delta(z)/\rho_w$), equations for the mean flow appear now with their usual form ($T^{ds} = 0$ and $\tau^{in} = 0$ in equations (9) and (10)), except for the Hasselmann force.

3.2. Turbulent Closure

[19] Equation (9) involves the divergence of the Reynolds stresses $\overline{\widehat{\mathbf{u}}'\widehat{w}'}$ that should now be computed or parameterized. We will use the turbulent closure model of *Craig and Banner* [1994]. It is a "level 2.5" turbulent closure scheme adapted from *Mellor and Yamada* [1982], with the dissipation of surface waves taken into account by introducing a near-surface injection of turbulent kinetic energy (TKE).

[20] The Reynolds stress is assumed to be linearly related to the shear: $\overline{\widehat{\mathbf{u}}'\widehat{w}'} = K_z \partial\mathbf{u}/\partial z$, with the eddy viscosity $K_z = lqS_m$, where $b = q^2/2$ is the TKE per unit mass, and l the mixing length. The later is parameterized as

$$l = \kappa(z_0 - z), \tag{12}$$

where $\kappa = 0.4$ is the von Kármán's constant and z_0 is a roughness length.

[21] The bottom has almost no effect on the near-surface dynamics, provided that the depth is substantially greater than the Stokes depth (see section 2.2) and the Ekman scale, which is $u_*/4f$ because the turbulent viscosity varies nearly linearly with depth [*Craig and Banner*, 1994]. Therefore the bottom boundary layer described by *Craig and Banner* [1994] is not described here.

[22] The equation for the evolution of TKE is

$$\frac{\partial b}{\partial t} = \frac{\partial}{\partial z}\left(lqS_q \frac{\partial b}{\partial z}\right) + lqS_m\left(\left(\frac{\partial \widehat{u}}{\partial z}\right)^2 + \left(\frac{\partial \widehat{v}}{\partial z}\right)^2\right) - \frac{q^3}{Bl} - \varphi^{ds}(z), \tag{13}$$

where S_m, S_q, and B are model constants for which the appropriate values are 0.39, 0.2, and 16.6. $\widehat{u}$, and $\widehat{v}$ are the components of the quasi-Eulerian velocity $\widehat{\mathbf{u}}$.

[23] The TKE evolution comes from a transport term ($\frac{\partial}{\partial z}\left(lqS_q \frac{\partial b}{\partial z}\right)$), a production term by the shear of the mean flow $\left(lqS_{\mathbf{m}}\left(\left(\frac{\partial \widehat{u}}{\partial z}\right)^2 + \left(\frac{\partial \widehat{v}}{\partial z}\right)^2\right)\right)$, a dissipation term ($\frac{q^3}{Bl}$), and a wave-induced source term ($\varphi^{ds}(z)$). The transport term is parameterized by the eddy diffusivity lqS_q.

[24] The conversion of wave kinetic and potential energy into TKE is the nonviscous wave "dissipation" Φ_{oc} (per unit mass and unit surface) of the wave field,

$$\Phi_{oc} = g \int S^{ds}(k,\theta) dk d\theta. \tag{14}$$

S^{ds} is distributed over depth as

$$\int_{-H}^{0} \varphi^{ds}(z) dz = \Phi_{oc}. \tag{15}$$

[25] Alternatively, Φ_{oc} may be prescribed as a surface flux of TKE and parameterized by $\Phi_{oc} = \alpha u_*^3$ with $\alpha \simeq 100$, consistent with the known loss of energy from the waves [*Craig and Banner*, 1994]. How the prescription as a surface flux modifies the TKE profiles will be studied in section 4.1. The consequences of neglecting the variations of α with the wave age (from 50 for young waves and fully developed waves to 150 otherwise) will be dealt with in section 4.3.

[26] The boundary condition for the TKE is then

$$\left. lqS_q \frac{\partial b}{\partial z}\right|_{z=0} = \alpha u_*^3, \tag{16}$$

which closes the model.

[27] We will now focus our attention on the steady state solutions, when wind- and wave-induced inertial oscillations are damped. The sea state is again modeled by *Kudryavtsev et al.*'s [1999] spectrum. It is assumed that the wave field is locally uniform even if the sea is not fully developed. In other words, the gradients of the radiation stresses are supposed much smaller than the leading terms in the momentum balance that are the Coriolis force, the Hasselmann force and the vertical mixing (see *Ardhuin et al.* [2004a] for a discussion of the impact of the radiation stress tensor in fetch limited conditions).

4. Model Results and Validation

4.1. Calibration of the Model With Observed Profiles of TKE Dissipation

[28] Two parameters remain unknown in this model: the roughness length z_0 and the scale α of the surface flux of

TKE. Practically, α may come from a wave model, and it is therefore supposed to be known [e.g., *Janssen et al.*, 2004], whereas z_0 is determined from measurements of TKE dissipation near the surface.

[29] In terms of TKE the surface layer can be divided into a "production layer" and a "diffusion layer" [*Craig and Banner*, 1994]. In the deeper layer the TKE equation is dominated by shear production and dissipation. Closer to the surface, the TKE balance is between diffusion from the surface flux and dissipation. One important modification brought by the present model to the one of Craig and Banner is the addition of the Stokes-Coriolis effect (the Hasselmann force). This effect modifies the Eulerian velocities over the whole water column (see section 4.2), but in the diffusion layer, the TKE production due to the shear of the mean flow has no importance. Therefore the TKE is expected to remain unchanged near the surface by the addition of the Stokes-Coriolis term. The numerical model results confirm this expectation, with relative changes in the magnitude of q less than 2% near the surface.

[30] As a result, we can rely on previous works without the Stokes-Coriolis effect, providing a parameterization of z_0 based on measurements of TKE dissipation ϵ in the diffusion layer. *Terray et al.* [1996] proposed a scaling of the roughness length with the significant wave height H_s. It comes from the physical hypothesis that the surface mixing is proportional to the height of the breaking waves, which can be evaluated by H_s. Other scalings of z_0, linked to the wind speed or to the friction velocity, are reported to fail [e.g., *Soloviev and Lukas*, 2003] because of no explicit dependence on the wave development. *Terray et al.* [2000] used the model of *Craig and Banner* [1994] to fit z_0, using dissipation data from several field experiments with various stages of wave development [*Drennan et al.*, 1996]. They found $z_0 = 1.6\ H_s$. As was pointed out by the authors, the model does not fit very well the data at depths of the order of H_s. Therefore they proposed a modified length scale which seems to fit better the observations. However, if we attempt a Lagrangian interpretation of their Eulerian measurements, there is water between their uppermost data points and the surface where TKE dissipation also occurs. Even if we suppose that ε decays linearly from $2\Phi_{oc}/H_s$ at $z = -H_s$ to Φ_{oc}/H_s at $z = 0$, the vertically integrated dissipation rate given by *Terray et al.* [2000, Figure 1], between the surface and $-H_s$, is greater than the wave input flux Φ_{oc} of TKE. This cannot be explained by the production of TKE by the shear of the mean flow, which is negligible near the surface. Besides, a decrease of ε between $z = -H_s$ and the surface is not supported by the Lagrangian averaged data of *Soloviev and Lukas* [2003]. The data and the modified mixing length given by *Terray et al.* [2000] are not compatible unless evidence is shown of a very small dissipation rate between $z = -H_s$ and the surface. Therefore we do not take the modified form of the mixing length, as done by *Mellor and Blumberg* [2004], but stick to (12). *Soloviev and Lukas* [2003] also used measurements of dissipation to estimate z_0 and found $z_0 = 0.6\ H_s$. However, the contribution of swell to the significant wave height was not evaluated, which may have lead to an underestimation of the ratio z_0/H_s.

[31] As the TKE equilibrium near the surface is between injection, dissipation and diffusion, one may wonder if a better representation of injection may not improve the model. The external source of TKE is the dissipation S^{ds} of the wave field, which is, in the case of a wind sea, due to breaking S^{break} and wave-turbulence interactions S^{turb}. The viscous dissipation, which is negligible, does not constitute a source of TKE. The separation between breaking and turbulence effects is not simple, but these two effects probably yield different depths of TKE injection, which can modify the profiles of TKE and of TKE dissipation.

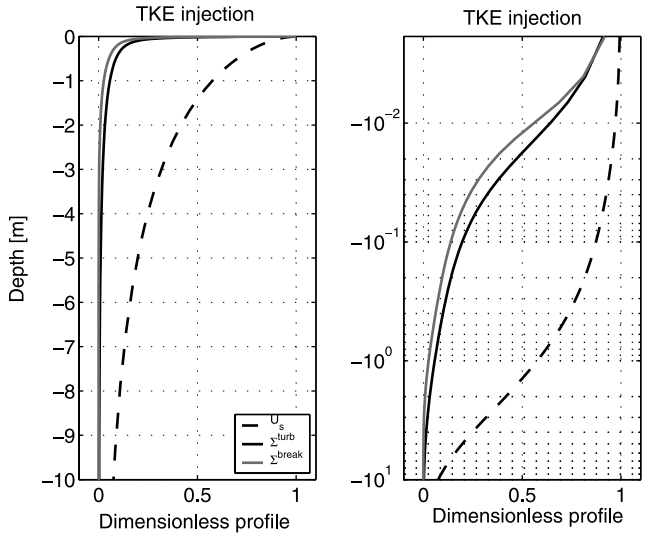

Figure 3. Profiles of normalized injection of turbulent kinetic energy (TKE) by wave breaking $\sum^{break}(z) = \varphi^{break}(z)/\varphi^{break}(z=0)$ and by interactions with turbulence $\sum^{turb}(z) = \varphi^{turb}(z)/\varphi^{turb}(z=0)$ in the case of fully developed waves with a wind of $U_{10} = 10\ \mathrm{m\ s^{-1}}$. Also shown is the profile of the Stokes drift $\mathbf{U}_s(z)/\mathrm{U}_s(z=0)$.

[32] *Teixeira and Belcher* [2002] used rapid distortion theory to derive an expression for the production of TKE due to interactions between turbulence and high-frequency waves,

$$\varphi^{turb}(z) = \overline{\widehat{\mathbf{u}}'\widehat{w}'}\partial\mathbf{U}_s/\partial z. \tag{17}$$

Using Lagrangian average of the Reynolds-averaged Navier-Stokes equations, *Ardhuin and Jenkins* [2006] extended this expression to low-frequency waves with the assumption that the turbulent fluxes are not correlated with the wave phases. The same expression was used in different studies of Langmuir circulations [e.g., *McWilliams et al.*, 1997], this time derived from the equations of *Craik and Leibovich* [1976]. The resulting profile of TKE injection follows the profile of $\partial\mathrm{U}_s/\partial z$ since the momentum flux is often more uniform than U_s over the Stokes depth, which is typically smaller than the Ekman depth. The use of a spectral distribution of waves leads to a profile of $\partial\mathrm{U}_s/\partial z$ much more sheared at the surface than the profile of U_s, whereas the use of a monochromatic wave would strongly overestimate the depth of injection of TKE (see Figure 3). It follows from this calculation that

$$\Phi_{oc}^{turb} \simeq \overline{\widehat{u}'\widehat{w}'}\mathrm{U}_s(z=0) \simeq 10 \times u_*^3, \tag{18}$$

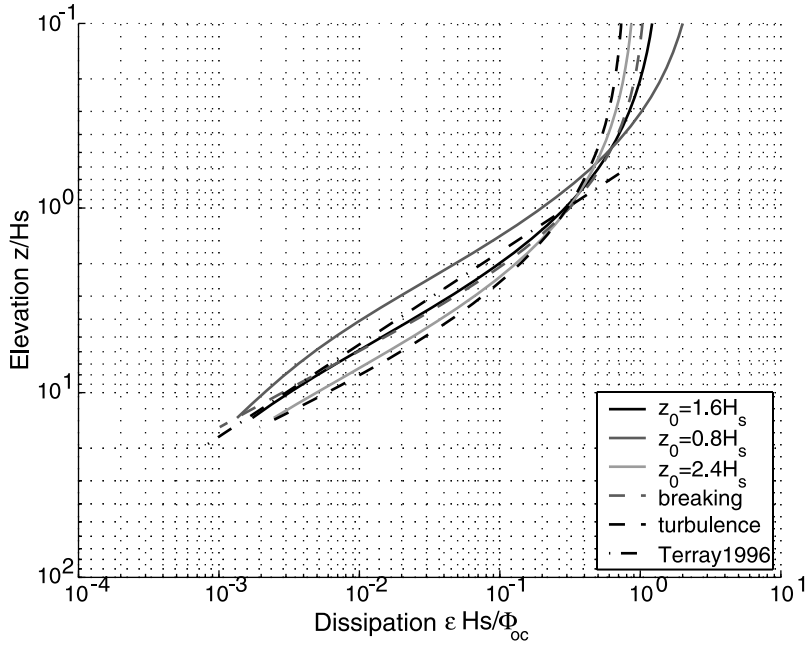

Figure 4. Normalized dissipation as a function of normalized depth, using the scaling of *Terray et al.* [2000]. $\Phi_{oc} = \alpha u_*^3$ is the surface flux of TKE. Curves correspond to different values of the roughness length z_0. The effect of injection of TKE over depth is also shown, with $\varphi(z) = \varphi^{break}(z)$, following the profile of *Sullivan et al.* [2004] and with $\varphi(z) = \varphi^{turb}(z)$, following the profile of $\partial U_s/\partial z$. Also shown is the result found by *Terray et al.* [1996].

which is around 10% of $\Phi_{oc} = \alpha u_*^3$. That means that the dissipation of the waves by interactions with turbulence is only 10% of the total waves dissipation. However, the correlations between wave groups and enhanced breaking [*Banner et al.*, 2000] may lead to a greater fraction of the total dissipation.

[33] In the case of dissipation by breaking, an injection over a certain depth linked to the wavelength of the breaking wave may be more realistic. *Sullivan et al.* [2004] proposed a profile for the injection of momentum by a breaking wave based on the laboratory data of *Melville et al.* [2002]. That profile can be approximated, after integration over time and horizontal dimensions of their breaker, by

$$f(z) = 4.227\left(1+\frac{5z}{\lambda}\right)^2 \exp\left(-5\left(\frac{5z}{\lambda}\right)^2\right). \tag{19}$$

With this expression most of momentum of breaking waves is released between the surface and a depth of $\lambda/5$, where λ is the wavelength of the breaking wave. We will suppose that, for a given wavelength, the injection of TKE and momentum follow the same depth profiles. To determine which waves are breaking, we will determine the spectral distribution of dissipation, as done by *Donelan* [1998], by supposing that the predominant terms in equation (1) are the input and the dissipation,

$$S^{in} + S^{ds} = 0, \tag{20}$$

which is formally valid only at the peak of the wave spectrum. Then the spectral distribution of dissipation can be obtained from S^{in}. The formulation of *Makin and Kudryavtsev* [1999] is, neglecting the sheltering effect of *Hara and Belcher* [2002],

$$S^{in} = \int \beta(k,\theta)E(k,\theta)dkd\theta, \tag{21}$$

with

$$\beta = 32\frac{\rho_a}{\rho_w}\left(1-1.3\left(\frac{c}{U_{10}}\right)^5\right)\left(\frac{u*}{c}\right)^2\cos(\theta)|\cos(\theta)|. \tag{22}$$

Using (19)–(22) provides an estimation of $\varphi^{break}(z)$.

[34] The appropriate surface boundary condition is now a zero flux of TKE, $lqS_q\partial b/\partial z = 0$. Figure 3 shows the profiles of φ^{ds} assuming that the dissipation of wave field comes entirely from breaking ($\varphi^{ds} = \varphi^{break}$) or entirely from wave-turbulence interactions ($\varphi^{ds} = \varphi^{turb}$). Both profiles are concentrated near the surface, much more so than the Stokes drift. A realistic case would be that wave dissipation comes from both phenomena with a ratio of the order of 20% for the wave-turbulence interactions ($\varphi^{ds} = 0.8\varphi^{break} + 0.2\varphi^{turb}$). Resulting profiles of dissipation are shown in Figure 4, as well as profiles of dissipation with surface flux of TKE and different values of the roughness length.

[35] As expected, in the extreme case of total dissipation due to wave-turbulence interactions, the TKE penetrates deeper which leads to more uniform dissipation profiles. The effect of depth injection is comparable to an increase of the roughness length. This is also true for the momentum, when the surface source is distributed over depth (not shown). The roughness length, which is fitted to measure-

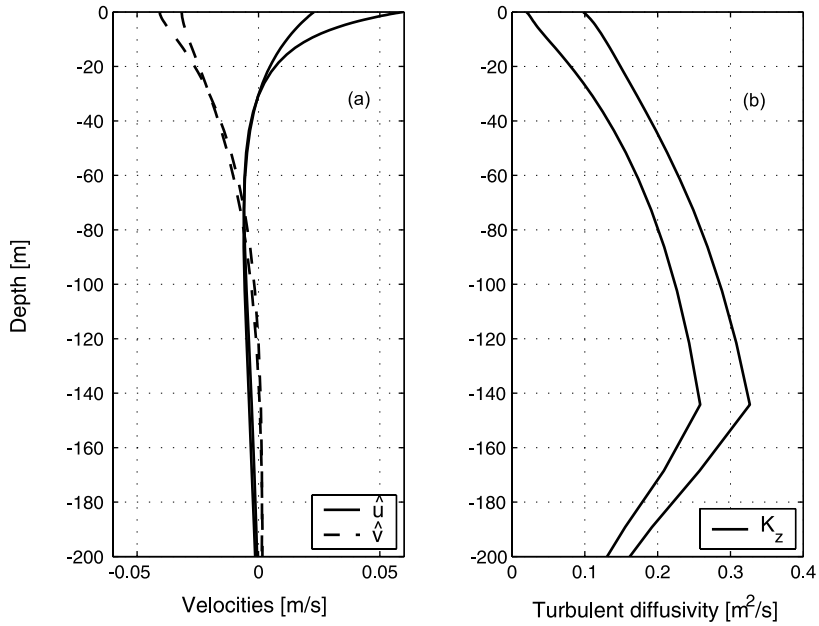

Figure 5. Evolution of profiles with an increasing fetch (wave heights from 0.6 m at 10 km offshore to the fully developed value 2.5 m) where (a) quasi-Eulerian velocity profiles become more uniform and (b) turbulent viscosity increases. The wind is set to U_{10} = 10 m s^{-1}, and the water depth is 300 m.

ments of dissipation, is supposed to take this effect into account. It can be seen from Figure 4 that a surface roughness at least of the order of H_s is needed, even if all the TKE is deeply injected with the profile of $\partial U_s/\partial z$.

4.2. Eulerian Hodographs and Shears

[36] The most obvious effect of waves on the mean flow is the enhancement of mixing. This effect gets stronger as waves become developed, because the roughness length is proportional to the wave height. Figure 5 shows the expected difference between a young sea (wave age C_p/U_{10} = 0.46) and a fully developed sea (C_p/U_{10} = 1.25).

[37] Another effect, in appearance less important, comes from the Stokes-Coriolis term. We can compute this effect by subtracting the results of the quasi-Eulerian current $\widehat{\mathbf{u}}'$ from model without the Hasselmann force to the results of the full model $\widehat{\mathbf{u}}$. This net contribution $\delta\mathbf{u} = \widehat{\mathbf{u}} - \widehat{\mathbf{u}}'$ of the Hasselmann force for the quasi-Eulerian velocity is shown in Figure 6. *Polton et al.* [2005] made a detailed analysis of the impact of this Stokes-Coriolis term on the profile of $\widehat{\mathbf{u}}$, with constant and linearly varying eddy viscosities. They

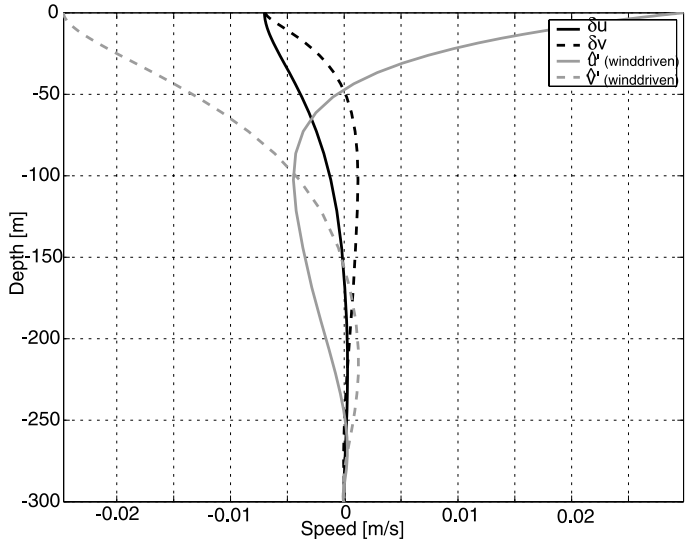

Figure 6. Quasi-Eulerian velocities driven by the wind stress $\widehat{\mathbf{u}}'$ and the Hasselmann force $\delta\mathbf{u} = \widehat{\mathbf{u}} - \widehat{\mathbf{u}}'$. Velocities are computed from the model without the Hasselmann force and from the full model minus the model without the Hasselmann force, respectively. The wind is set to U_{10} = 10 m s^{-1}, and the sea is developed (fetch > 1000 km).

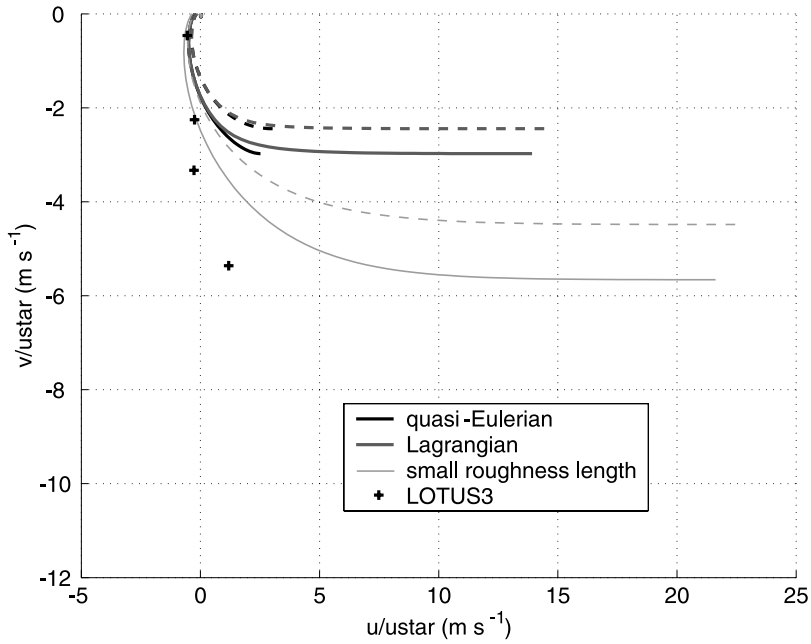

Figure 7. Hodographs of quasi-Eulerian and Lagrangian velocity. Curves are for $u_* = 8.3 \times 10^{-3}$ m s^{-1} and a fully developed sea (H_s = 1.6 m). Also shown is the mean profile from LOTUS3 [*Price and Sundermeyer*, 1999] at 5, 10, 15, and 25 m and, for comparison with the findings of *Polton et al.* [2005], the Eulerian current from the model with a small surface mixing (small roughness length $z_0 = 1.6 \times 10^{-3}$ m). Solid curves are model results with the Hasselmann force, and dashed curves are results without the Hasselmann force.

showed that the detailed profile of the Stokes drift does not matter as soon as the Ekman depth is much larger than the Stokes depth. In this case, they showed that the contribution of the Hasselmann force is similar to the addition of a surface stress to the right of the wind, with a magnitude related to the Stokes transport $\mathbf{M}^w$. This is also true in our model since we are considering an unstratified water column (large Ekman depth) and a wind sea (small Stokes depth). Using a full spectrum to compute the Stokes drift is not important when looking at the Stokes-Coriolis effect on the quasi-Eulerian velocity $\widehat{\mathbf{u}}$. Eulerian velocities spiral in an Ekman fashion, and vanish at a depth given by the Ekman depth $u^*/4f$. The Hasselmann force has thus an influence much deeper than the Stokes drift [*Xu and Bowen*, 1994]. Because the transport induced by this Stokes-Coriolis term is equal to the Stokes transport [*Hasselmann*, 1970], an estimation of the importance of this effect is the ratio of the Stokes transport to the Ekman transport (Figure 2), which can be more than 30% for midlatitudes. Substantial modifications at the surface (20%) and over the whole water column (30% at 100 m) are found in the case of a developed sea (Figure 6).

[38] *Lewis and Belcher* [2004] and *Polton et al.* [2005] studied the impact of the Stokes-Coriolis term on the Eulerian Ekman spiral with an unstratified water column and with an eddy viscosity that varies linearly with depth. They reported that this Stokes-Coriolis term could explain the tendency of the spiral to be shifted in the direction opposite to the wind as observed in some field experiments, such as LOTUS3 [*Price and Sundermeyer*, 1999]. We must notice that they took small values of z_0, of the order of 1 cm. Such values are commonly used in order to fit surface drift observations (see section 4.3) with the Eulerian surface current (around 3% of the wind speed U_{10}, e.g., $q = 0.03$ [*Lewis and Belcher*, 2004, Table 3]). The present model was used to simulate conditions observed during the LOTUS3 experiment. The model mixing K_z is enhanced by breaking ($z_0 \simeq 2.5$ m), which leads to quasi-Eulerian currents near the surface much reduced compared to the findings of *Polton et al.* [2005] (less than 1% of the wind speed U_{10} (Figure 7)). *Polton et al.* [2005] reported minor changes of velocity in the bulk of the Ekman layer to the values of z_0, but they used $z_0 \simeq 1$ cm, which is 2 orders of magnitude below the values of the present model. Also, it is the near-surface dynamics within the first 10 m that are of interest here, and they are quite sensitive to values of z_0 larger than 1 m, as pointed out by *Craig and Banner* [1994, section 5], because of a very large increase in K_z. Therefore the good agreement found by *Lewis and Belcher* [2004] and by *Polton et al.* [2005] for the uppermost current 2 m ($z = -5$ and $z = -10$ m (Figure 7)) is not obtained with the present model. The value of the crosswind component of the model's velocity is only 50% of the observed value at $z = -5$ m. If the subsurface deflection of the quasi-Eulerian velocity due to the Stokes-Coriolis effect is still significant, the vertical profiles and velocity spiral are more different from the observations than with the models of *Lewis and Belcher* [2004] and *Polton et al.* [2005]. This misfit may be explained by the stratification: The mixed layer was only 10–25 m thick during LOTUS3 [*Price and Sundermeyer*, 1999], with a strong diurnal cycling.

[39] *Terray et al.* [2000] compared the results of the Craig and Banner model (without the Stokes-Coriolis term) to quasi-Eulerian velocity profiles and shears obtained with a

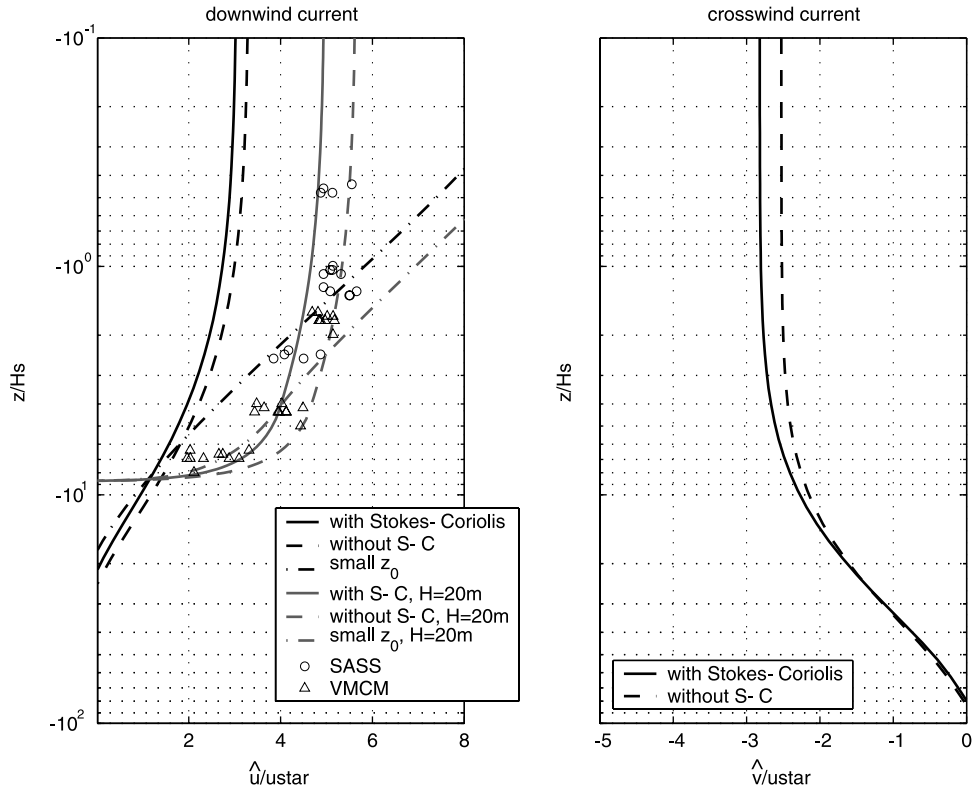

Figure 8. Downwind and crosswind quasi-Eulerian currents. Curves correspond to U_{10} = 13.6 m s^{-1} and a fetch of 100 km (H_s = 2.3 m). Solid and dashed curves show model results with and without the Hasselmann force, respectively. The data from the buoy (SASS) and the mooring (VMCM) of *Terray et al.* [2000, Figure 3] are plotted with markers. As the water column was stratified during these measurements (thermocline at 20 m depth), we also show, for qualitative comparison for the downwind component, the model results with a water depth of 20 m. Dash-dotted curves are model results without the Hasselmann force and with a small roughness length $z_0 = 0.05 \times H_s$.

wave follower much closer the surface [*Santala and Terray*, 1992]. The addition of the Stokes-Coriolis term does not substantially modify the shear, but the magnitude of the currents is modified. However, the field data used by *Terray et al.* [2000] were obtained with relatively young waves ($C_p/U_{10} \simeq 0.74$) so that currents driven by the Hasselmann force are 1 order of magnitude smaller than currents driven by the wind. Therefore this data set is not ideal for highlighting the Stokes-Coriolis effect (Figure 8). A data set with fully developed waves would have been more useful for that purpose. Moreover, the water column was stratified below 20 m depth. Therefore the present comparison of their data and the model remains qualitative. However, roughness length 1 order of magnitude smaller than H_s is clearly not compatible with this data set.

[40] *McWilliams et al.* [1997] used large eddy simulations (LES) to study the impacts of Langmuir circulations (LCs) on the mixed layer in a weakly stratified case. They did not take surface wave breaking into account but they used an input of TKE, given by the shear of the Stokes drift (17). Some comparison can be made between our present model with a simple turbulent closure scheme and their LES results: In particular, *McWilliams et al.* [1997, Figure 2] computed the impact of the Hasselmann force on the Eulerian current [*Hasselman et al.*, 1973]. We must notice that their Stokes transport (a monochromatic wave of H = 2.3 m and λ = 60 m) is 4 times larger than expected at full development (they use U_{10} = 5 m s^{-1}). In their case, the Ekman transport and the Stokes transport are of the same order. Figure 9 shows the present model results using the same Stokes drift used by *McWilliams et al.* [1997] and a Stokes drift from developed waves with U_{10} = 5 m s^{-1}. These results are similar to the LES experiment, except for the u component in the near-surface region that is much more uniform in their case. In spite of a close agreement between their bulk eddy viscosity and our eddy viscosity, the mixing due to LCs is significantly different to the one of our simple model. *Kantha and Clayson* [2004] used an intermediately complex turbulence closure model based on two equations for q^2 and $q^2 l$ and simulated the same LES experiment. As they noticed, their model also underestimated the near-surface mixing of the Langmuir cells.

4.3. Lagrangian Drift

[41] The mean drift velocity $\mathbf{U}$ is the sum of the quasi-Eulerian flow $\hat{\mathbf{u}}$, computed with the model described above, and the Stokes drift $\mathbf{U}_s$. Now considering the net wave-induced mass transport, the Stokes-Coriolis term is of prime importance. In terms of mass transport in the downwind direction, that term creates an Eulerian return flow which compensates the Stokes transport, leading to a zero wave-induced transport in steady conditions given by equation (9)

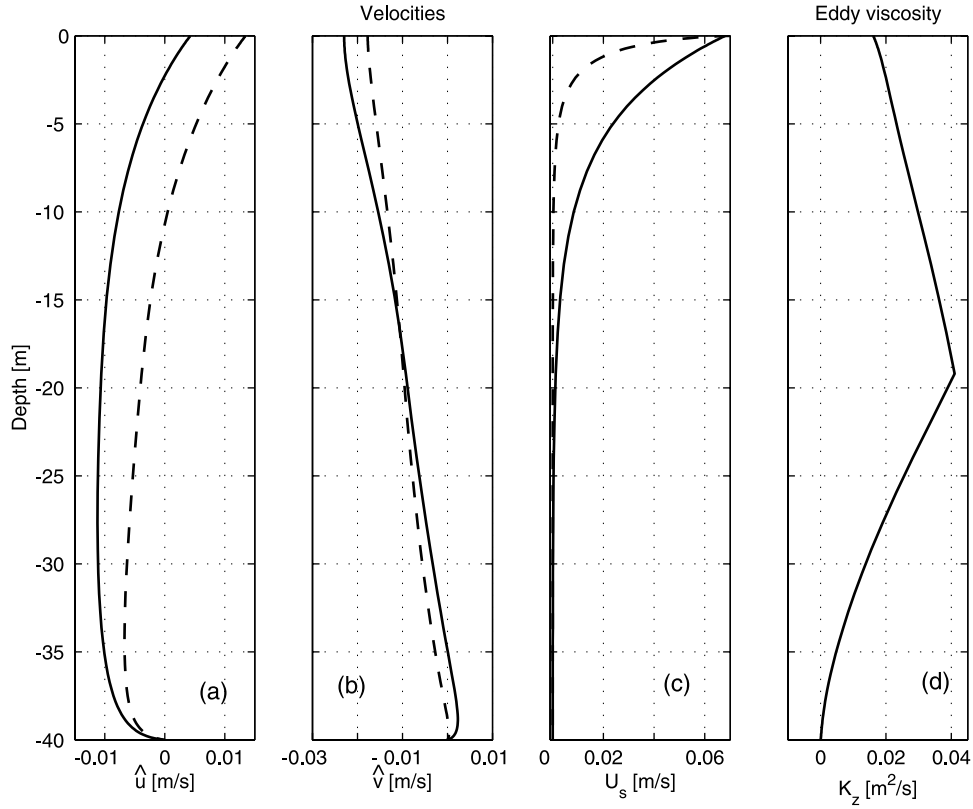

Figure 9. Profiles of quasi-Eulerian velocity components (a) $\widehat{u}$ and (b) $\widehat{v}$, (c) Stokes drift $\mathbf{U}_s$, and (d) eddy viscosity K_z. Curves are for $U_{10} = 5$ m s^{-1}. Solid curves show results with the Stokes drift of a monochromatic wave as used by *McWilliams et al.* [1997], and dashed curves show results for a fully developed sea with this wind ($H_s = 0.9$ m).

[see also *Hasselmann*, 1970]. Because turbulence diffuses vertically the momentum source that is the Hasselmann force, the return flow is less sheared than the Stokes drift. Therefore the return flow does not compensate the Stokes drift near the surface, and overcompensates it below. Instead of quasi-Eulerian and Lagrangian, Figure 10 shows a decomposition into quasi-Eulerian current driven by the wind $\widehat{\mathbf{u}}'$ and Stokes drift plus quasi-Eulerian current driven by the Hasselmann force $\mathbf{U}_s + \delta\mathbf{u} = \mathbf{U}_s + \widehat{\mathbf{u}} - \widehat{\mathbf{u}}'$.

[42] It can be seen that near the surface the downwind drift in the present model is essentially due to the Stokes drift (at least 80%), for fully developed waves. A simple calculation takes the surface drift to be the sum of the usual Ekman Eulerian current (i.e., from an ocean circulation model without the Stokes-Coriolis term) plus the Stokes drift [e.g., *Annika et al.*, 2001]. This simplification leads to slight overestimations (less than 5%) of the surface drift for fully developed waves. For very young waves the Eulerian current is of same order as the Stokes drift but the Hasselmann force is reduced so that its effect can also be neglected in terms of surface drift.

[43] In the crosswind direction the wave-induced drift is the quasi-Eulerian current due to the Stokes-Coriolis stress. Although the total transport is zero in this direction, the velocity is not zero at each depth, leading to a small wave-induced drift to the right of the wind near the surface and to the left below (see Figure 6 and section 4.2). The mean wind-induced drift of a water particle at the surface is not well known. *Huang* [1979] reviewed field and laboratory experiments about surface drift of water, ice, oil, and objects, but laboratory experiments or floating objects observations are not supposed to give the same drift as water particles in the presence of developed waves. The different results are scattered roughly around 3% of the wind speed U_{10}. *Churchill and Csanady* [1983] studied Lagrangian motions of drogues and drifters and found surface drifts between 2 and 2.5% of the wind speed U_{10}. The present model yields smaller velocities, around 1.5%.

[44] This ratio of 1.5% does not vary much with fetch (Figures 11 and 12). For shorter fetches, the Stokes drift is small and the Eulerian velocity is larger, thanks to a small mixing (Figure 12, dotted curves). Note that we computed the Stokes drift for very short fetches with *Kudryavtsev et al.*'s [1999] spectrum, whereas this spectrum is not expected to behave correctly for such young seas (B. Chapron, personal communication, 2004). The effect of the dependence of the atmospheric roughness length with the sea state is also shown: A wind-wave coupling represented by (couplage Donelan) is used instead of the Charnock relation (6). This coupling leads to an increase of the surface stress for young seas, and thus to a increase of the Eulerian current (dash-dotted curves). Furthermore, the TKE flux is $\Phi_{oc} = \alpha u_*^3$, where α is also known to depend on the wave age. We use here an analytical fit to the distribution of α as a function of c_p/u_{*a} [*Terray et al.*, 1996, Figure 8]; α can be taken around 60 for very young waves (age $Cp/u_{*a} \simeq 5$).

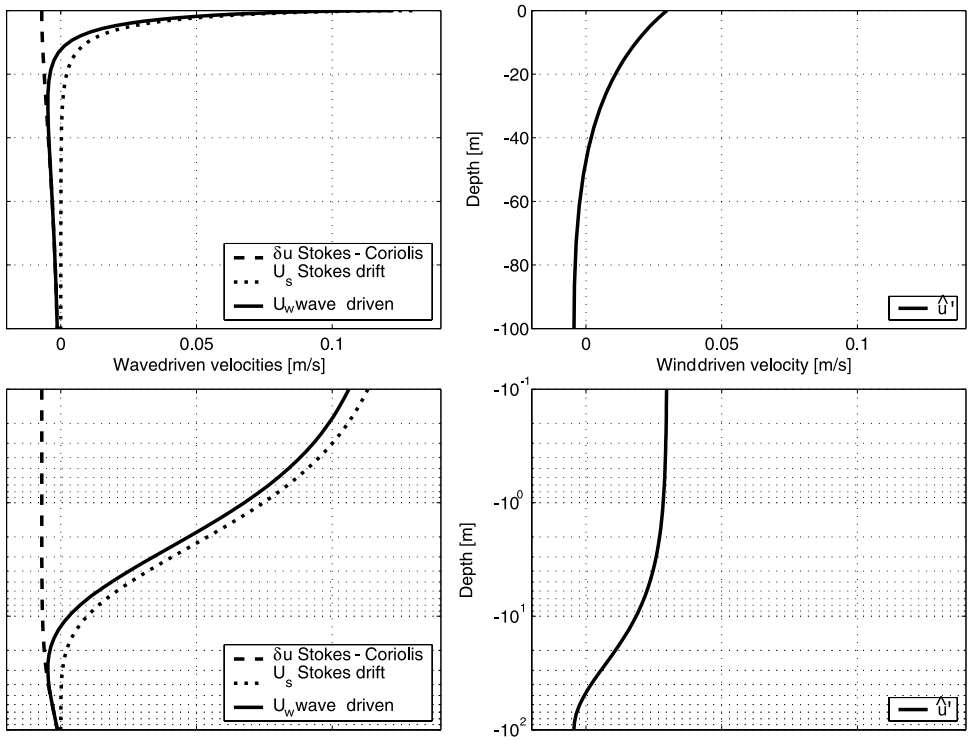

Figure 10. Details of the velocity profiles in the downwind direction. (left) Lagrangian drift induced by wave mass transport $\mathbf{U}_w$, equal to Stokes drift U_s plus quasi-Eulerian current driven by the Hasselmann force $\delta u = \hat{u} - \hat{u}'$. (right) Wind-driven quasi-Eulerian current (i.e., the model result without the Stokes-Coriolis term) $\hat{u}'$. Figure 10 (left) plus Figure 10 (right) (i.e., $U_w + \hat{u}' = U_s + \delta u + \hat{u}'$) gives the total Lagrangian velocity U. Curves are for $U_{10} = 10$ m s^{-1} and fully developed waves (fetch superior to 1000 km). Figure 10 (bottom) is shown on a logarithmic scale.

It increases to 180 for developing waves ($10 < Cp/u_{*a} < 20$), and then decreases to 80 for fully developed waves ($Cp/u_{*a} \simeq 30$). As this effect slightly reduces the mixing for very young waves and for fully developed waves, the quasi-Eulerian current at the surface slightly increases. It is the contrary for developing waves, for which the mixing is slightly enhanced (Figure 12, solid curves). However, it is the increase of the roughness length z_0 that dominates the evolution of the near-surface mixing with wave development as expected by *Craig and Banner* [1994],

$$K_z \propto u_* \alpha^{1/3} z_0^{0.8} (z_0 - z)^{0.2}. \tag{23}$$

[45] The Lagrangian surface drift appears to be almost independent of the fetch (Figure 11). This drift strongly depends on the depth because of the vertical shear of the Stokes drift (and also, for short fetches, to the shear of the quasi-Eulerian current).

5. General Discussion

[46] Clearly, the surface drift is more sensitive to the surface mixing of the model than to the Stokes-Coriolis term. Near-surface profiles are, as pointed out by *Craig and Banner* [1994], strongly dependent on the roughness length. However, if the scaling of *Terray et al.* [1996] is valid (that is, z_0 and H_s are of the same order, which is confirmed by observations), then the uncertainty on the quasi-Eulerian velocity is not that large. A much smaller roughness length like $z_0 = 0.6\ H_s$, as prescribed by *Soloviev and Lukas* [2003], leads to Eulerian surface currents 1.5 times larger than with the present value $z_0 = 1.6\ H_s$. In terms of Lagrangian surface drift, the underestimation would be smaller, from 10% for long fetches to 20% for short fetches. Thus a hopefully more physically sound definition for z_0, such as an average size of breaking waves, is not expected to give significant differences in drift.

[47] Although there is a reasonable agreement between the present model and quasi-Eulerian velocity shears measured by *Santala and Terray* [1992], there is a large difference between predictions of Lagrangian drift and drifter observations. It is possible that a second-order approximation may not be accurate enough for steep waves, and wave-wave interactions (modulations) may enhance the Stokes drift in a random wave field. *Melsom and Sæatra* [2004] have included fourth-order terms in their estimation of the Stokes drift for monochromatic waves, but the effect of these terms is typically less that 10% of the second-order terms, even for the steepest waves. It is more likely that turbulent structures associated with breaking fronts may contribute to the drift at the surface, and need to be parameterized.

[48] Breaking wave fronts may cover an area of the order of a few percent of the sea surface. One may use empirically derived distributions $\Lambda(C)dC$ for the length of breaking crest with a phase speed between C and $C + dC$ per unit area

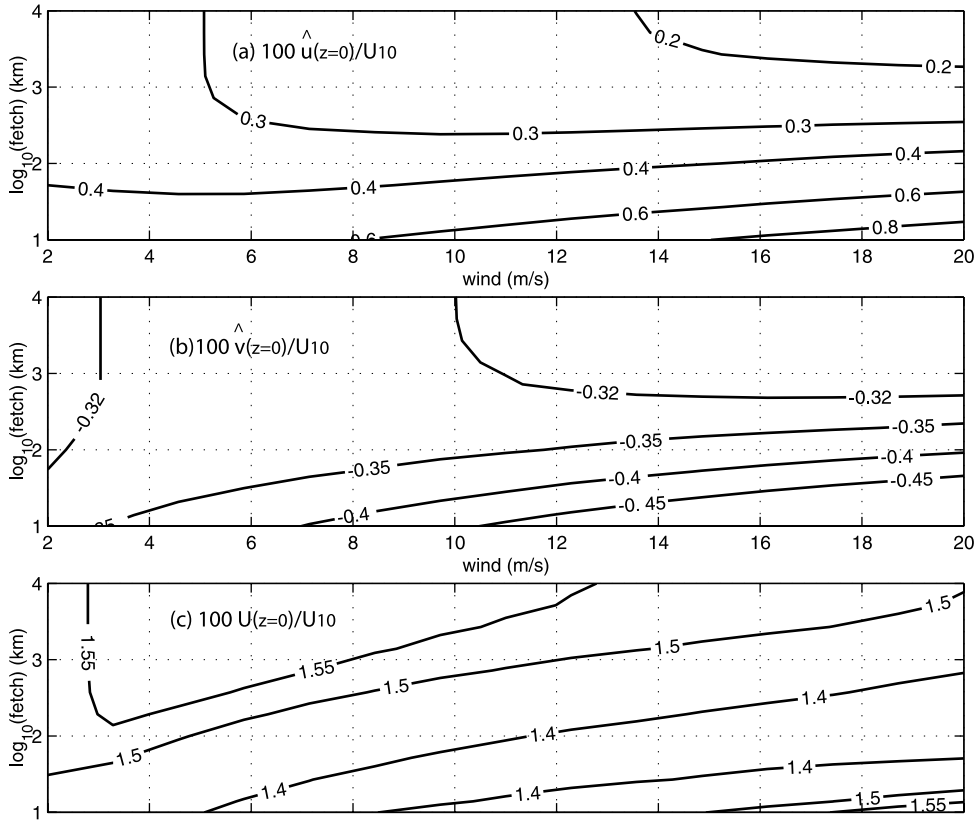

Figure 11. (a) Quasi-Eulerian current downwind $\hat{u}$, (b) crosswind $\hat{v}$, and (c) total Lagrangian drift $|\hat{\mathbf{u}} + \mathbf{U}_s$ at the surface as a function of wind speed and fetch. The results are shown as percentages of the wind speed U_{10}. The wind-wave coupling (equation (7)) and an estimation of α as a function of the wave age are used.

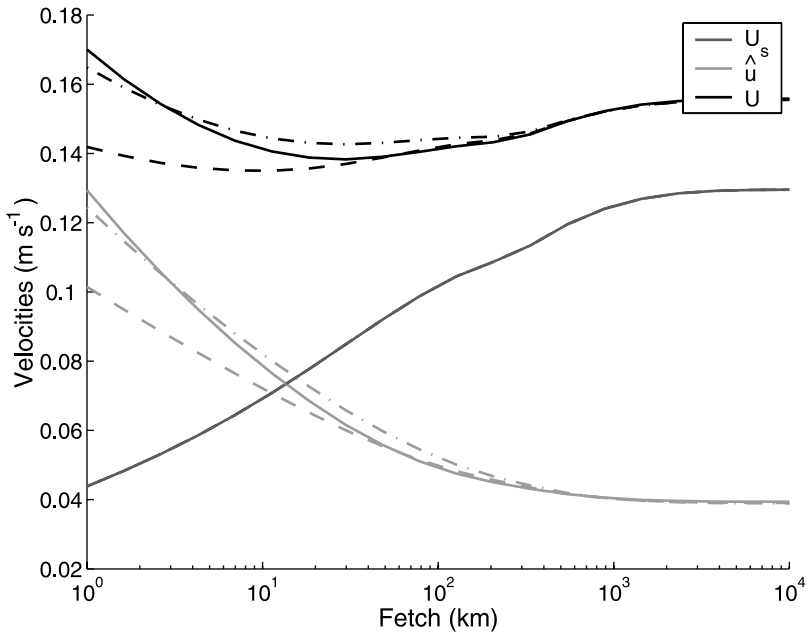

Figure 12. Quasi-Eulerian drift $|\hat{\mathbf{u}}|$, Stokes drift U_s, and total drift $U = |\hat{\mathbf{u}} + \mathbf{U}_s$ at the surface as a function of fetch. We show model results Charnock's formula and a TKE flux $\Phi_{oc} = \alpha u_*^3$ with $\alpha = 100$ (dashed curves), using the coupling as done by *Donelan* [1998] and $\alpha = 100$ (dash-dotted curves), or using the coupling as done by *Donelan* [1998] and a variable α from *Terray et al.* [1996] (solid curve). The wind is set to $U_{10} = 10$ m s^{-1}.

[*Melville and Matusov*, 2002], one finds that objects randomly distributed at the surface of the ocean will have an extra drift of

$$\overline{u} = \int LC\Lambda(C)dC, \tag{24}$$

with L the displacement at the passage of a breaker. Since breakers propagate at a speed of about 0.8 C and the breaker lifetime is about the wave period $T = 2\pi C/g$, one finds that $\overline{u}$ is of the order of 6×10^{-3} m s^{-1} for $U_{10} = 10$ m s^{-1}, and this velocity increases with the cube of the wind speed. Therefore this effect may become significant for large wind speeds, but it only affects depths down to a small fraction of the wavelength, typically a few percent [*Melville et al.*, 2002]. This calculation only includes transient large-scale breakers. Microscale breakers, with a relatively longer lifetime, may yield a larger contribution.

[49] The other turbulent structures that are likely to account for most of the discrepancy between observed drift speeds and the model are the Langmuir circulations. These structures extend down to the base of the mixed layer and have been repeatedly observed as soon as the wave and winds are steady enough that the cells can develop, even in shallow water [e.g., *Marmorino et al.*, 2005]. LCs are characterized by strong variations Δu of the downwind velocity with maxima associated with convergence zones at the surface. Δu is reported to be of the order of 1–3% of the wind speed by *Smith* [1998]. As a slightly buoyant object would tend to be trapped in the convergence zones, it can easily drift with a mean velocity larger than the actual mean by 1% of the wind speed. This "Langmuir bias" could thus be the principal reason why measured drift velocities are larger than given by the present model, and also larger than the HF-radar measurements by *Dobson et al.* [1989]. Langmuir circulations further raise the issue of the adequacy of the turbulent closure with a $k - l$ model to model mixing due to such organized vortices created by wave-current interactions. Recent studies [e.g., *Noh et al.*, 2004] have investigated Langmuir circulations with large eddy simulations that do not use such a simple closure scheme. However, these studies still need to be validated with field observations such as those of *Smith* [1999].

[50] Finally, the impact of a density stratification can be included in the present model. A reduced mixed layer depth leads to an increase of the quasi-Eulerian velocity because the Ekman transport is conserved. As shown in Figure 8, it may increase the quasi-Eulerian velocity by a factor of 2 or 3, which would be significant also in terms of Lagrangian surface drift.

6. Conclusion

[51] We presented here a model of a uniform and homogeneous ocean driven by wind and associated waves. Distinction is made between wave motion, including the Stokes drift, and a quasi-Eulerian motion, driven by the momentum flux from atmosphere, by the Coriolis force and by the Hasselmann force (also called "Stokes-Coriolis effect"). The waves are supposed to be a linear superposition of monochromatic components which satisfy the usual dispersion relation. The sea state is thus modeled by a directional spectrum of sea surface elevation variance. The Stokes drift and the vertically integrated Stokes transport are respectively the third and first moments of the frequency spectrum, and are therefore sensitive to the high-frequency part of the spectrum, i.e., the short waves. Thus a spectrum designed for remote sensing applications (fitted to reproduce the fourth moment of the spectrum) is supposed to give reasonable results for the Stokes drift calculation. This Stokes drift is found to be around 1.2% of the wind speed U_{10}, and the corresponding Stokes transport around 20–30% of the Ekman transport at midlatitudes, for developed waves. The use of a monochromatic wave cannot represent well the surface drift value, the vertically integrated transport, and the depth involved.

[52] The wave field influences the quasi-Eulerian motion via two different effects: The Stokes drift, in a rotating frame, creates the Hasselmann force, which drives an Eulerian return flow to compensate the Stokes transport. The presence of waves also increases the near-surface mixing. A simple turbulent closure scheme gives an eddy viscosity that can be used to represent the latter effect. The roughness length for this closure scheme is evaluated according to observations of TKE dissipation near the surface. The model result is then examined and we can summarize it by comparison to the near-surface physics of most ocean circulation models (OCMs), which use small mixing at the surface (represented here by a small roughness length $z_0 < 0.1$ m). (1) A surface mixing at least 1 order of magnitude greater than in current OCMs (and dependent on the sea state) seems realistic. Significant consequences on the sea surface temperature are expected [*Mellor and Blumberg*, 2004]. (2) As a consequence of this strong mixing, there is a strong reduction of the vertical shear of the quasi-Eulerian velocity near the surface (see Figure 13). (3) However, Lagrangian drift velocity is highly sheared due to because of the shear of the Stokes drift near the surface (see Figure 13), leading to near-surface profiles quite close to those of the Eulerian current in some OCMs. (4) Although observations of surface drift and comparisons with the wind speed are not very reliable, an important part of the surface drift of objects may be still missing in the present formulation. The "Langmuir bias," which is the correlation of surface convergence and increased velocity, should explain some of this missing drift, as well as the stratification which was not taken into account. (5) The Hasselmann force has a significant impact in terms of vertical profiles of Eulerian velocities (this force leads to current magnitudes of 20–30% of the magnitude of currents driven by the wind stress). This impact is relatively small on the surface Lagrangian drift, which could be approximated by the sum of the Stokes drift plus the Eulerian current driven only by the wind stress. (6) In terms of Lagrangian drift at different depth, stationary waves create a mass transport in the wind-wave direction near the surface and in the opposite direction below until a depth of the order of the Ekman depth. If properties are homogeneously distributed in this surface layer then wave transport can be ignored. Otherwise it should be computed. (7) For really young seas, as it happens in some costal areas or lakes, the near-surface dynamics are closer to that described by traditional OCMs, with a small Stokes drift and a relatively weak mixing.

[53] In conclusion, the surface drift and mixing cannot be understood without the waves. However, there still are very few data sets that are complete. The reason is that fields

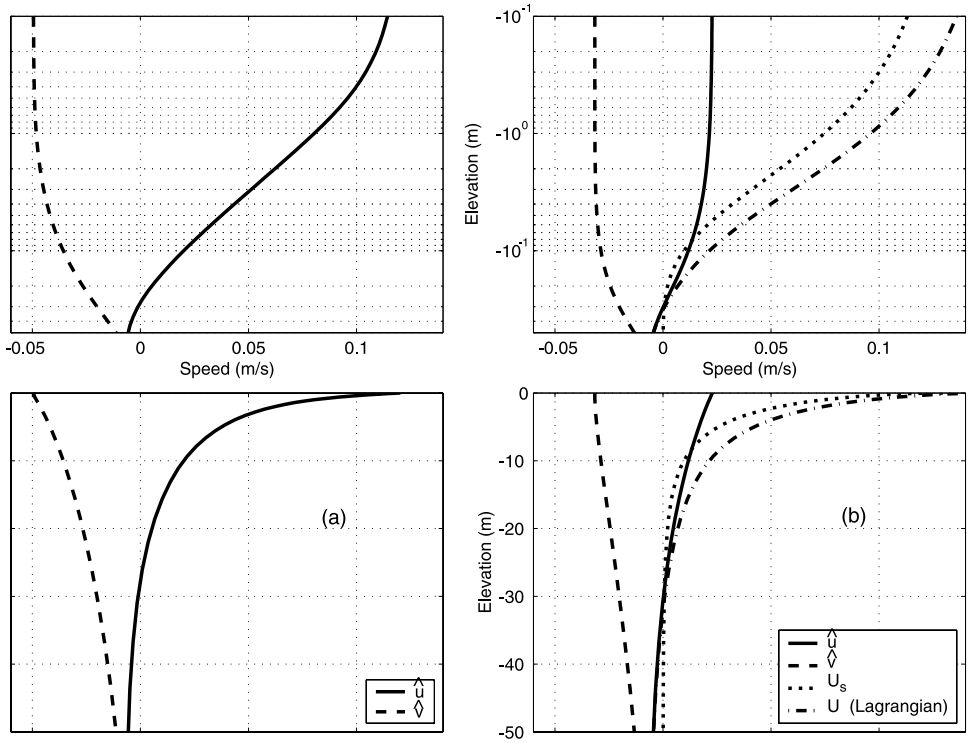

Figure 13. Velocity profiles for $U_{10} = 10$ m s^{-1} and fully developed waves. (a) Quasi-Eulerian velocity from the model without Stokes-Coriolis effect and with $z_0 = 0.1$ m, which represents a small surface mixing in an ocean circulation model. (b) Quasi-Eulerian velocity, Stokes drift, and Lagrangian velocity from the model with the Stokes-Coriolis effect and $z_0 = 1.6 \times H_s = 4.5$ m. Figures 13a (top) and 13b (top) are shown on a logarithmic scale.

experiments on Ekman currents or mixed layers and studies on waves are rarely made simultaneously. Furthermore, near-surface Lagrangian, Eulerian or quasi-Eulerian averaging are often significantly different but hardly well identified. The present study demonstrates the need for more near-surface measurements to gather all this information.

[54] **Acknowledgments.** The initial version of the computer code for the mixed layer model was kindly provided by P. Craig and M. L. Banner. Many discussions with B. Chapron, N. Reul, V. Kudryavtsev, A. D. Jenkins, and P. Daniel were helpful in understanding several issues addressed in this paper.

References

Agrawal, Y. C., E. A. Terray, M. A. Donelan, P. A. Hwang, A. J. Williams, W. Drennan, K. Kahma, and S. Kitaigorodskii (1992), Enhanced dissipation of kinetic energy beneath breaking waves, *Nature*, *359*, 219–220.

Alves, J. H. G. M., and M. L. Banner (2003), Performance of a saturation-based dissipation-rate source term in modeling the fetch-limited evolution of wind waves, *J. Phys. Oceanogr.*, *33*, 1274–1298.

Andrews, D. G., and M. E. McIntyre (1976), Planetary waves in horizontal and vertical shear: The generalized Eliassen-Palm relation and the mean zonal acceleration, *J. Atmos. Sci.*, *33*(11), 2031–2048.

Andrews, D. G., and M. E. McIntyre (1978), An exact theory of nonlinear waves on a Lagrangian-mean flow, *J. Fluid Mech.*, *89*, 609–646.

Annika, P., T. George, P. George, N. Konstantinos, D. Costas, and C. Koutitas (2001), The Poseidon operational tool for the prediction of floating pollutant transport, *Mar. Pollut. Bull.*, *43*, 270–278.

Ardhuin, F. (2005), Etat de la mer et dynamique de l'océan superficial (in French), Ph.D. thesis, 318 pp., Université de Bretagne Occidentale, Brest, France.

Ardhuin, F., and A. D. Jenkins (2006), On the interaction of surface waves and upper ocean turbulence, *J. Phys. Oceanogr*, in press.

Ardhuin, F., B. Chapron, and T. Elfouhaily (2004a), Waves and the air-sea momentum budget: Implications for ocean circulation modeling, *J. Phys. Oceanogr.*, *34*, 1741–1755.

Ardhuin, F., F.-R. Martin-Lauzer, B. Chapron, P. Craneguy, F. Girard-Ardhuin, and T. Elfouhaily (2004b), Dérive à la surface de l'océan sous l'effet des vagues, *C. R. Geosci.*, *336*, 1121–1130.

Ardhuin, F., A. D. Jenkins, D. Hauser, A. Reniers, and B. Chapron (2005), Waves and operational oceanography: Toward a coherent description of the upper ocean for applications, *Eos Trans. AGU*, *86*(4), 37–39.

Banner, M. L., and W. L. Peirson (1998), Tangential stress beneath wind-driven air-water interfaces, *J. Fluid Mech.*, *364*, 115–145.

Banner, M. L., A. V. Babanin, and I. R. Young (2000), Breaking probability for dominant waves on the sea surface, *J. Phys. Oceanogr.*, *30*, 3145–3160.

Bleck, R. (2002), An oceanic general circulation model framed in hybrid isopicnic-cartesian coordinates, *Ocean Modell.*, *4*, 55–88.

Charnock, H. (1955), Wind stress on a water surface, *Q. J. R. Meteorol. Soc.*, *81*, 639–640.

Churchill, G. H., and G. T. Csanady (1983), Near-surface measurements of quasi-Lagrangian velocities in open water, *J. Phys. Oceanogr.*, *13*, 1669–1680.

Cox, C., and W. Munk (1954), Measurement of the roughness of the sea surface from photographs of the Sun's glitter, *J. Opt. Soc. Am.*, *44*(11), 838–850.

Craig, P. D., and M. L. Banner (1994), Modeling wave-enhanced turbulence in the ocean surface layer, *J. Phys. Oceanogr.*, *24*, 2546–2559.

Craik, A. D. D., and S. Leibovich (1976), A rational model for Langmuir circulations, *J. Fluid Mech.*, *73*, 401–426.

Dobson, F., W. Perrie, and B. Toulany (1989), On the deep water fetch laws for wind-generated surface gravity waves, *Atmos. Ocean*, *27*, 210–236.

Donelan, M. A. (1998), Air-water exchange processes, in *Physical Processes in Lakes and Oceans*, *Coastal Estuarine Stud.*, vol. 54, edited by J. Imberger, pp. 18–36, AGU, Washington, D. C.

Donelan, M. A., J. Hamilton, and W. H. Hui (1985), Directional spectra of wind-generated waves, *Philos. Trans. R. Soc. London, Ser. A*, *315*, 509–562.

Drennan, W. M., M. A. Donelan, E. A. Terray, and K. B. Katsaros (1996), Oceanic turbulence dissipation measurements in SWADE, *J. Phys. Oceanogr.*, *26*, 808–815.

Drennan, W. M., H. C. Graber, D. Hauser, and C. Quentin (2003), On the wave age dependence of wind stress over pure wind seas, *J. Geophys. Res.*, *108*(C3), 8062, doi:10.1029/2000JC000715.

Ekman, V. W. (1905), On the influence of the Earth's rotation on ocean currents, *Ark. Mat. Astron. Fys.*, *2*, 1–53.
Elfouhaily, T., B. Chapron, K. Katsaros, and D. Vandemark (1997), A unified directional spectrum for long and short wind-driven waves, *J. Geophys. Res.*, *102*, 15,781–15,796.
Garrett, C. (1976), Generation of Langmuir circulations by surface waves: A feedback mechanism, *J. Mar. Res.*, *34*, 117–130.
Gelci, R., H. Cazalé, and J. Vassal (1957), Prévision de la houle: La méthode des densités spectroangulaires, *Bull. Inf. Com. Oceanogr. Etud. Cotes*, *9*, 416–435.
Groeneweg, J. (1999), Wave-current interactions in a generalized Lagrangian mean formulation, Ph.D. thesis, Delft Univ. of Technol., Delft, Netherlands.
Groeneweg, J., and G. Klopman (1998), Changes in the mean velocity profiles in the combined wave-current motion described in GLM formulation, *J. Fluid Mech.*, *370*, 271–296.
Hara, T., and S. E. Belcher (2002), Wind-forcing in the equilibrium range of wind-wave spectra, *J. Fluid Mech.*, *470*, 223–245.
Hasselmann, K. (1970), Wave-driven inertial oscillations, *Geophys. Fluid Dyn.*, *1*, 463–502.
Hasselmann, K., et al. (1973), Measurements of wind-wave growth and swell decay during the Joint North Sea Wave Project, *Dtsch. Hydrogr. Z.*, *8*(12), 1–95.
Hristov, T., C. Friehe, and S. Miller (1998), Wave-coherent fields in air flow over ocean waves: Identification of cooperative turbulence behavior buried in turbulence, *Phys. Rev. Lett.*, *81*(23), 5245–5248.
Huang, N. E. (1979), On surface drift currents in the ocean, *J. Fluid Mech.*, *91*, 191–208.
Janssen, P. (2004), *The Interaction of Ocean Waves and Wind*, 300 pp., Cambridge Univ. Press, New York.
Janssen, P. A. E. M., O. Saetra, C. Wettre, and H. Hersbach (2004), Impact of the sea state on the atmosphere and ocean, *Ann. Hydrogr.*, *3*(772), 1–23.
Jenkins, A. D. (1987), Wind and wave induced currents in a rotating sea with depth-varying eddy viscosity, *J. Phys. Oceanogr.*, *17*, 938–951.
Kantha, L. H., and C. A. Clayson (2004), On the effect of surface gravity waves on mixing in the oceanic mixed layer, *Ocean Modell.*, *6*, 101–124.
Kenyon, K. E. (1969), Stokes drift for random gravity waves, *J. Geophys. Res.*, *74*, 6991–6994.
Komen, G. J., L. Cavaleri, M. Donelan, K. Hasselmann, S. Hasselmann. and P. A. E. M. Janssen (1994), *Dynamics and Modeling of Ocean Waves*, Cambridge Univ. Press, New York.
Kudryavtsev, V. N., V. K. Makin, and B. Chapron (1999), Coupled sea surface–atmosphere model: 2. Spectrum of short wind waves, *J. Geophys. Res.*, *104*, 7625–7639.
Lange, B., H. K. Johnson, S. Larsen, J. Højtrup, H. Kofoed-Hansen, and M. J. Yelland (2004), On detection of a wave age dependency for the sea surface roughness, *J. Phys. Oceanogr.*, *34*, 1441–1458.
Lewis, D. M., and S. E. Belcher (2004), Time-dependent, coupled, Ekman boundary layer solutions incorporating Stokes drift, *Dyn. Atmos. Oceans*, *37*, 313–351.
Longuet-Higgins, M. S. (1967), Action of a variable stress at the surface of water waves, *Phys. Fluids*, *12*(4), 737–740.
Makin, V. K., and V. N. Kudryavtsev (1999), Coupled sea surface–atmosphere model: 1. Wind over waves coupling, *J. Geophys. Res.*, *104*, 7613–7623.
Marmorino, G. O., G. B. Smith, and G. J. Lindemann (2005), Infrared imagery of large-aspect-ratio Langmuir circulation, *Cont. Shelf Res.*, *25*, 1–6.
McIntyre, M. E. (1981), On the "wave momentum" myth, *J. Fluid Mech.*, *106*, 331–347.
McIntyre, M. E. (1988), A note on the divergence effect and the Lagrangian-mean surface elevation in periodic water waves, *J. Fluid Mech.*, *189*, 235–242.
McWilliams, J. C., P. P. Sullivan, and C.-H. Moeng (1997), Langmuir turbulence in the ocean, *J. Fluid Mech.*, *334*, 1–30.
Mellor, G. (2003), The three-dimensional current and surface wave equations, *J. Phys. Oceanogr.*, *33*, 1978–1989.
Mellor, G., and A. Blumberg (2004), Wave breaking and ocean surface layer thermal response, *J. Phys. Oceanogr.*, *34*, 693–698.
Mellor, G. L., and T. Yamada (1982), Development of a turbulence closure model for geophysical fluid problems, *Rev. Geophys.*, *20*(4), 851–875.
Melsom, A., and Ø. Sæatra (2004), Effects of wave breaking on the near-surface profiles of velocity and turbulent kinetic energy, *J. Phys. Oceanogr.*, *34*, 490–504.
Melville, W. K., and P. Matusov (2002), Distribution of breaking waves at the ocean surface, *Nature*, *417*, 58–63.
Melville, W. K., F. Verron, and C. J. White (2002), The velocity field under breaking waves: Coherent structures and turbulence, *J. Fluid Mech.*, *454*, 203–233.
Noh, Y., H. S. Min, and S. Raasch (2004), Large eddy simulation of the ocean mixed layer: The effects of wave breaking and Langmuir circulation, *J. Phys. Oceanogr.*, *34*, 720–733.
Phillips, O. M. (1977), *The Dynamics of the Upper Ocean*, 336 pp., Cambridge Univ. Press, New York.
Pierson, W. J., Jr., and L. Moskowitz (1964), A proposed spectral form for fully developed wind seas based on the similarity theory of S.A. Kitaigorodskii, *J. Geophys. Res.*, *69*, 5181–5190.
Polton, J. A., D. M. Lewis, and S. E. Belcher (2005), The role of wave-induced coriolis-stokes forcing on the wind-driven mixed layer et al., *J. Phys. Oceanogr.*, *35*, 444–457.
Price, J. F., and M. A. Sundermeyer (1999), Stratified Ekman layers, *J. Geophys. Res.*, *104*, 20,467–20,494.
Santala, M. J., and E. A. Terray (1992), A technique for making unbiased estimates of current shear from a wave-follower, *Deep Sea Res., Part A*, *39*, 607–622.
Semtner, A. J. (1995), Modeling ocean circulation, *Science*, *269*, 1379–1385.
Smith, J. A. (1998), Evolution of Langmuir circulation during a storm, *J. Geophys. Res.*, *103*, 12,649–12,668.
Smith, J. A. (1999), Observations of wind, waves, and the mixed layer: The scaling of surface motion, in *The Wind-Driven Air-Sea Interface*, edited by M. L. Banner, pp. 231–238, Univ. of N. S. W., Sydney, Australia.
Snodgrass, F. E., G. W. Groves, K. Hasselmann, G. R. Miller, W. H. Munk, and W. H. Powers (1966), Propagation of ocean swell across the Pacific, *Philos. Trans. R. Soc. London, Ser. A*, *249*, 431–497.
Soloviev, A., and R. Lukas (2003), Observation of wave-enhanced turbulence in the near-surface layer of the ocean during TOGA COARE, *Deep Sea Res., Part I*, *50*, 371–395.
Spaulding, M. (1999), Drift current under the action of wind and waves, in *Wind-Over-Wave Couplings*, edited by S. G. Sajjadi, N. H. Thomas, J. C. R. Hunt, pp. 243–256, Clarendon, Oxford, U. K.
Sullivan, P. P., J. C. McWilliams, and W. K. Melville (2004), The oceanic boundary layer driven by wave breaking with stochastic variability. part 1. Direct numerical simulation, *J. Fluid Mech.*, *507*, 143–174.
Teixeira, M. A. C., and S. E. Belcher (2002), On the distortion of turbulence by a progressive surface wave, *J. Fluid Mech.*, *458*, 229–267.
Terray, E. A., M. A. Donelan, Y. C. Agrawal, W. M. Drennan, K. K. Kahma, A. J. Williams, P. A. Hwang, and S. A. Kitaigorodskii (1996), Estimates of kinetic energy dissipation under breaking waves, *J. Phys. Oceanogr.*, *26*, 792–807.
Terray, E. A., W. M. Drennan, and M. A. Donelan (2000), The vertical structure of shear and dissipation in the ocean surface layer, in *Proceedings of the Symposium on Air-Sea Interaction, Sydney*, pp. 239–245, Univ. of N. S. W., Sydney, Australia.
Thorpe, S. A., T. R. Osborn, D. M. Farmer, and S. Vagle (2003), Bubble clouds and Langmuir circulation: Observations and models, *J. Phys. Oceanogr.*, *33*, 2013–2031.
Wamdi Group (1988), The WAM model—A third generation ocean wave prediction model, *J. Phys. Oceanogr.*, *18*, 1775–1810.
Weber, J. E. (1981), Ekman currents and mixing due to surface gravity waves, *J. Phys. Oceanogr.*, *11*, 1431–1435.
White, B. S. (1999), Wave action on currents with vorticity, *J. Fluid Mech.*, *386*, 329–344.
Xu, Z., and A. J. Bowen (1994), Wave- and wind-driven flow in water of finite depth, *J. Phys. Oceanogr.*, *24*, 1850–1866.
Youssef, M., and M. Spaulding (1993), Drift current under the action of wind and waves, in *Proceedings of the Sixteenth Arctic and Marine Oil Spill Program Technical Seminar*, pp. 587–615, Environ. Can., Ottawa, Ontario.

F. Ardhuin and N. Rascle, Centre Militaire d'Océanographie, Service Hydrographique et Océanographique de la Marine, 13 rue du Chatellier, F-29609 Brest, France. (ardhuin@shom.fr; rascle@shom.fr)
E. A. Terray, Department of Applied Ocean Physics and Engineering, Woods Hole Oceanographic Institution, MS-11, 217 Bigelow, Woods Hole, MA 02543, USA. (eterray@whoi.edu)